



Effect of prior martensite on bainite transformation and microstructure of high-carbon nano-bainitic steel

Xin-pan Yu¹ · Hui-bin Wu^{1,2} · Yang Gu¹ · Rui Yuan¹ · You-you Zhang¹ · Yu-hui Feng¹

Received: 22 October 2020 / Revised: 28 December 2020 / Accepted: 28 December 2020 / Published online: 2 April 2021
© China Iron and Steel Research Institute Group 2021

Abstract

Bainite transformation kinetics, microstructure, and mechanical properties were comparably investigated by X-ray diffraction, scanning electron microscopy, electron backscatter diffraction, transmission electron microscopy observation, and tensile and impact tests for two treatments: with and without quenching before isothermal bainite transformation at 300 °C. Both the incubation time and growth stage of bainite transformation are accelerated by the introduction of prior martensite, especially the former. In addition, the bainite microstructure around the prior martensite is refined and shows a similar orientation with the martensite due to the strain field caused by the existence of prior martensite. The finer bainite microstructure and prior martensite improve the strength and hardness of the high-carbon nano-bainitic steel. Although the presence of prior martensite and low misorientation relationship between the martensite and the adjacent bainite microstructure are prejudicial to impact toughness, the nanoscale bainite microstructure can inhibit the crack propagation and then improve the impact toughness of the high-carbon nano-bainitic steel.

Keywords Nano-bainitic steel · Prior martensite · Transformation kinetics · Microstructure · Mechanical property

1 Introduction

Nano-bainitic steel, a typical representative of the new-generation advanced high strength steel, exhibits a remarkable combination of strength and toughness, and meets the requirement of high safety standard and weight reduction in automotive industry [1–3]. The excellent combination of mechanical properties appears to be partly due to the formation of nanostructured bainite microstructure which consists of fine bainitic ferrite plates with an average thickness of ~ 50 nm and retained austenite embedded between these plates [4]. Unlike other high strength steel [5, 6], the extremely strong and cheap nano-bainitic steel can be manufactured without expensive

alloying elements, rapid heat treatment, or complicated mechanical processing. Therefore, nano-bainitic steel has incredible potential in modern industry, such as transport, construction and offshore industries, as well as defense applications [7–9].

At first, the nano-bainitic steel was fabricated by isothermally holding at a low temperature with a duration up to days due to high-C content [10, 11]. Shortening the bainite transformation time has been achieved by optimizing alloy composition, including adding Co and Al elements [12, 13], and ausforming before isothermal transformation at low temperature [14, 15]. Many researches have shown that the nanostructured microstructure and mechanical properties of nano-bainitic steel are significantly influenced by austempering temperature [16–18]. The process of austempering below martensite start temperature (M_s) with or without ausforming has been conducted on nano-bainitic steels to accelerate the transformation and improve mechanical properties [19–21]. The results showed that the finer bainite microstructure and higher strength of nano-bainitic steel austempered below M_s are related to the higher transformation driving force and the presence of prior martensite.

✉ Hui-bin Wu
whbustb@163.com

¹ Collaborative Innovation Center of Steel Technology, University of Science and Technology Beijing, Beijing 100083, China

² Beijing Laboratory of Metallic Materials and Processing for Modern Transportation, University of Science and Technology Beijing, Beijing 100083, China

The acceleration of bainite transformation by prior martensite is mainly reflected in shortening the incubation time [22, 23]. However, there still exists the debate on the transformation acceleration mechanism by prior martensite. Someone considers that the strain or dislocations in austenite introduced by martensite transformation can accelerate the subsequent bainite transformation [22, 24], and the others believe that the martensite–austenite interface provides the nucleation sites for bainite microstructure [25]. In addition, there are few researches on the effect of prior martensite on the mechanical properties of high-carbon nano-bainitic steel.

The aim of the present paper is to quantitatively investigate the bainite transformation kinetics, microstructure, and mechanical properties of high-carbon nano-bainitic steels with or without prior martensite. The microstructure and mechanical properties of high-carbon nano-bainitic steel are observed and tested using the scanning electron microscope (SEM), transmission electron microscope (TEM), X-ray diffraction (XRD), and electron backscatter diffraction (EBSD), combined with tensile test and impact test.

2 Experimental

The chemical composition of the tested steel used in current paper is presented in Table 1. High content of Si element could improve the thermal stability of nano-bainite microstructure while inhibit the precipitation of cementite during isothermal transformation [26]. The addition of Mn element in steel could improve the hardenability, so that the supercooled austenite does not decompose into ferrite or pearlite during cooling process. The tested steel was melted in a vacuum induction furnace. After homogenizing at 1200 °C for ~ 2 h, the steel billet was hot-forged into square bars. Bainite start temperature (B_s) and M_s were measured to be ~ 426 and 190 °C by the dilatometric experiments. According to the heat treatment processes presented in Fig. 1, the transformation kinetics measurements were performed on a Bähr 805 A dilatometer to record the dilation during the cooling and isothermal transformation. Dilatometry specimens were machined from forged stock with a length of 10 mm and a diameter of 4 mm. For quenching and bainite transformation (QBT)

Table 1 Chemical composition of tested steel (wt.%)

C	Si	Mn	Al	Nb	S	P	Fe
0.70	2.47	1.46	0.87	0.022	0.003	0.006	Balance

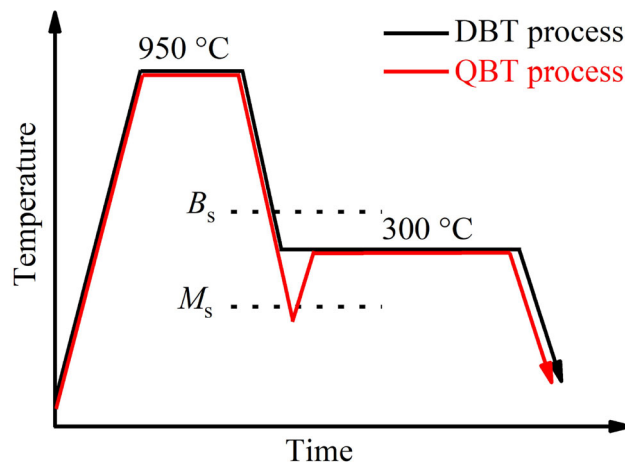


Fig. 1 Schematic diagram of heat treatment process

process, a specimen was austenitized at 950 °C for 30 min before rapid cooling down to 178 °C, then reheated up to 300 °C for isothermal transformation, and finally cooled to room temperature. There was no quenching treatment for direct bainite transformation (DBT) process, and a specimen was cooled from 950 to 300 °C for isothermal bainite transformation. The austempering time for both the processes is 2 h.

Tensile tests were carried out on an Instron CM75105 electromechanical tester at room temperature, with a crosshead speed of 3 mm/min. Tensile specimens with a thickness of 2.5 mm and a length of 50 mm were taken from the austempered specimens from DBT and QBT processes. According to ASTM E23, standard V-notched specimens with a size of 10 mm × 10 mm × 50 mm were used on impact tester at room temperature. For each process, three specimens were tested.

The morphology and crystallographic orientation of microstructure were characterized by SEM, TEM, and EBSD. Specimens for SEM observations were mechanically ground using silicon carbide paper from 200 to 2000 grit and then mechanically polished. The microstructures at low temperature were observed via a QUANTAFEG 450 SEM after the specimens were etched with 4 vol.% nitric acid solution. The morphology and size of bainite microstructure including bainitic ferrite plate and film-like retained austenite were examined using an FEIF 20 TEM. Specimens for TEM were mechanically cut into 500 μm slice and then ground down to 50 μm in thickness by abrasive paper. These specimens were electropolished at 50 V using a twin-jet unit with an electrolyte consisting of 5 vol.% perchloric acid, 15 vol.% glycerol, and 80 vol.% ethanol. Specimens for EBSD were electrochemically polished in perchloric acid alcohol solution with volume ratio of 4:1. EBSD measurements were performed using a JEOL JSM-6301F SEM operated at 20 kV with a step size

of 50 nm to investigate the crystallographic orientation relationship between martensite grain and the surrounding nano-bainite microstructure.

X-ray diffraction experiments were carried out using a D8 Advance diffractometer with a scanning rate of 0.05 (°)/min over the range $2\theta = 30^\circ\text{--}100^\circ$, and unfiltered Cu K α radiation was operated at 40 kV and 40 mA. Peak positions and widths of Bragg reflections were determined by a self-consistent profile fitting technique using the Pearson VII function. The fraction of retained austenite (V_γ) within the specimens was evaluated through the integrated intensities of (111), (200), (220), and (311) peaks of austenite and (110), (002), (112), and (022) peaks of ferrite. Compared to other alloying elements, the effect of carbon on the lattice parameter of retained austenite is more profound, so that the carbon content of retained austenite (C_γ) in the specimens prepared by both the processes was calculated using the following equation [27, 28]:

$$C_\gamma = (\alpha_\gamma - 0.035467)/0.00467 \quad (1)$$

where α_γ is the lattice parameter of retained austenite, nm.

3 Results and discussion

3.1 Transformation kinetics

The dilation–temperature curves, dilation–time curves, and transformation rate–time curves of DBT and QBT processes during the cooling and isothermal process are shown in Fig. 2. For both the processes, all dilations show linear relationship with temperature until cooling down to 178 °C (below M_s temperature) for QBT process or to 300 °C for DBT process, which indicates that no ferrite or pearlite transformation occurs in their intervals. These results can also be determined for the observation from the microstructure in Fig. 3. The same linear variation can be observed during cooling down to room temperature from isothermal temperature for both the processes, suggesting that the retained austenite does not decompose into martensite as shown in the dashed square box (Fig. 2a). The obvious isothermal time-dependent dilations can be observed when cooling down to 300 °C and holding isothermally at this temperature for DBT and QBT processes.

The corresponding dilation–time curves (Fig. 2b) clearly show that the isothermal transformation for 2 h is enough for bainite transformation at 300 °C for both the processes. For DBT process, the dilation–time curve shows a significant incubation period followed by an explosive expansion when holding at the isothermal temperature. By contrast, it is observed that isothermal bainite

transformation occurs as soon as the holding temperature is reached, almost without an incubation platform observed for QBT process. The incubation time for bainite transformation was calculated to be about 702.0 s for DBT process and 57.6 s for QBT process, respectively, which is consistent with the result about the acceleration bainite transformation by prior martensite [29]. Beside the shorter incubation time, the time for bainite transformation (from the beginning of isothermal process to the finishing of bainite transformation) for QBT process is also shorter than that for DBT process. The time node when the isothermal holding ceases represents the finishing of bainite transformation, as determined by the tangential line method on the dilation–time curve. The finishing time for bainite transformation was estimated to be about 5011.3 s for DBT process and 4046.4 s for QBT process, respectively, as shown in Fig. 2b.

It has been proved that bainite transformation can be accelerated by the formation of martensite before isothermal holding and that the kinetics of the martensite and bainite transformation were analyzed by being combined with microstructure characterization [22, 29–31]. The transformation rate–time curves for DBT and QBT processes holding at 300 °C are shown in Fig. 2c. In QBT process, not only the maximum transformation rate is higher than that of DBT process, but that in QBT process appears earlier than that in DBT process. Both the nucleation period and the growth stage of bainite transformation were shortened by the formation of prior martensite in present paper. This finding is inconsistent with the previous results that the acceleration effect of prior martensite is mainly reflected in shortening incubation period rather than in the following transformation process. Hence, the bainite transformation acceleration mechanism by the prior martensite needs to be investigated through microstructural analysis.

3.2 Microstructure

Figure 3a, b shows SEM and TEM micrograph of bainite microstructure formed at 300 °C by DBT process. The bainite microstructure consists of bainitic ferrite (BF) plates and retained austenite (RA) with film-like and blocky morphology. Short-range diffusion of carbon atoms from bainitic ferrite plate to adjacent film-like austenite occurs. The blocky retained austenite cannot transform into martensite during the further cooling process due to carbon enrichment within the blocky RA in isothermal bainite transformation [32]. This microstructural result is consistent with the dilation–temperature shown in Fig. 2a.

Figure 3c, d shows the microstructure of the specimen obtained through QBT process. The microstructure consists of lenticular prior martensite (PM) and nano-scaled bainite

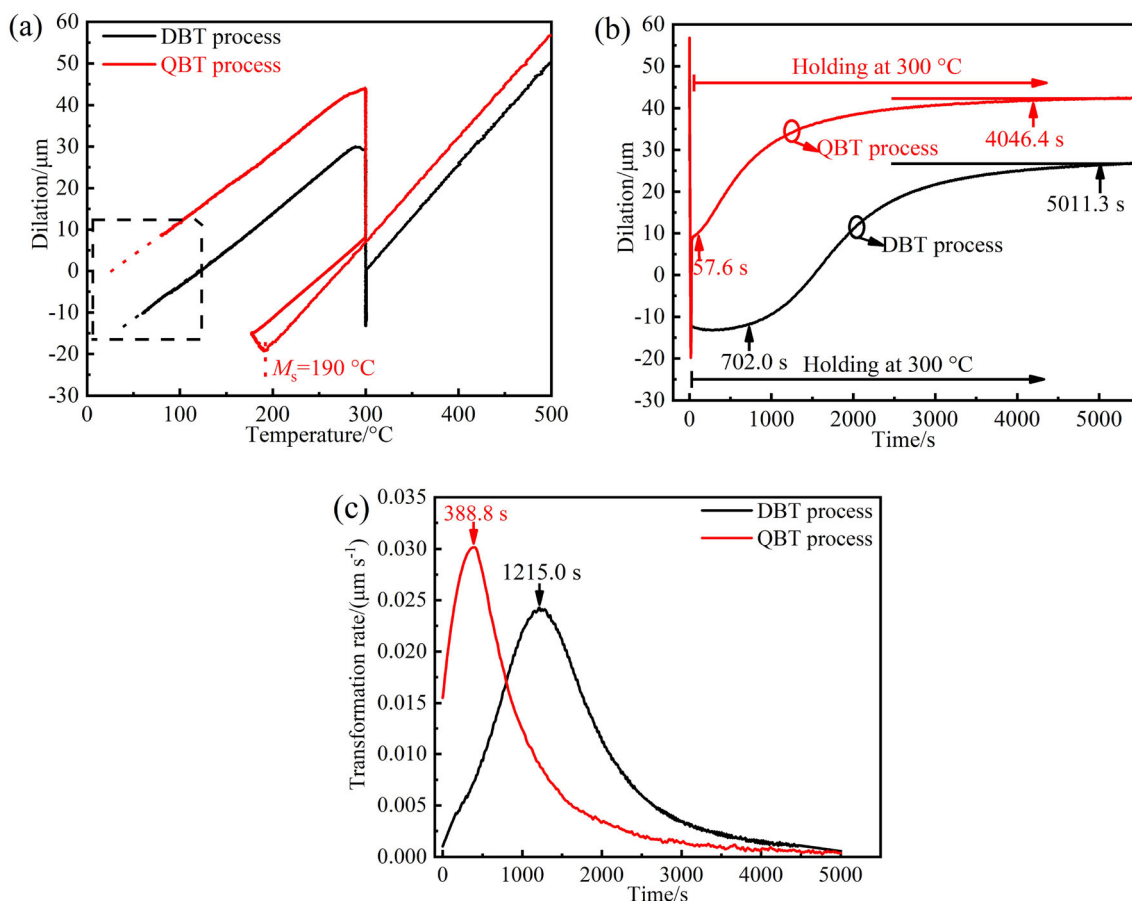


Fig. 2 Dilation–temperature curves (a), dilation–time curves (b) and transformation rate–time curves (c) of DBT and QBT processes during cooling and isothermal transformation

microstructure including BF plates and RA. Compared to those within the specimen obtained by DBT process, the amount and size of blocky retained austenite are smaller in the specimen manufactured through QBT process. It is worth noting that there are carbide-free bainitic ferrite plates with two different thicknesses observed in the specimen (Fig. 4d), indicating two distinct nucleation sites.

In order to quantitatively investigate the effect of prior martensite on bainite microstructure, the true thickness of bainitic ferrite plates (t) is defined according to the equation $\bar{L}_T = \pi t/2$ rather than $\bar{L} = 2t$, due to the fact that the mean linear intercept \bar{L}_T , determined from a direction normal to the plate length, is easier to be measured than that measured along random orientation \bar{L} . The nanostructured bainitic ferrite in the specimen obtained by DBT process nucleates at austenite grain boundary and internal defects, i.e., dislocation debris, and eventually grows into thicker and uniform plates, as shown in Fig. 3b. The average thickness of the bainitic ferrite plates in this specimen is 106.9 ± 2.9 nm by measuring about 10 TEM micrographs. By contrast, the thickness of the bainitic ferrite plates in the specimen obtained by QBT process

shows bimodal distribution. The average thickness of bainitic ferrite plates around prior martensite grain is 43.4 ± 1.1 nm, whereas that away from prior martensite grain is 119.4 ± 4.9 nm. The thickness of bainitic ferrite plates away from martensite is like that in the specimen fabricated by DBT process, indicating that the thicker bainitic ferrite plates in the specimen obtained by QBT process also nucleate at austenite grain boundary or internal defects. However, the presence of prior martensite refines the adjacent bainite microstructure.

XRD patterns of the specimens treated by DBT and QBT processes are shown in Fig. 4. The volume fraction of retained austenite and average carbon content within it can be calculated through XRD patterns. The volume fraction of prior martensite from 10 SEM micrographs through Image-Pro Plus software is 12.6%, which is consistent with the results (12.3%) calculated by Koistinen–Marburger equation [33]:

$$f_i^M = 1 - \exp\{-1.1 \times 10^{-2}(M_s - T_Q)\} \quad (2)$$

where f_i^M is the volume fraction of prior martensite; and T_Q is the quenching temperature.

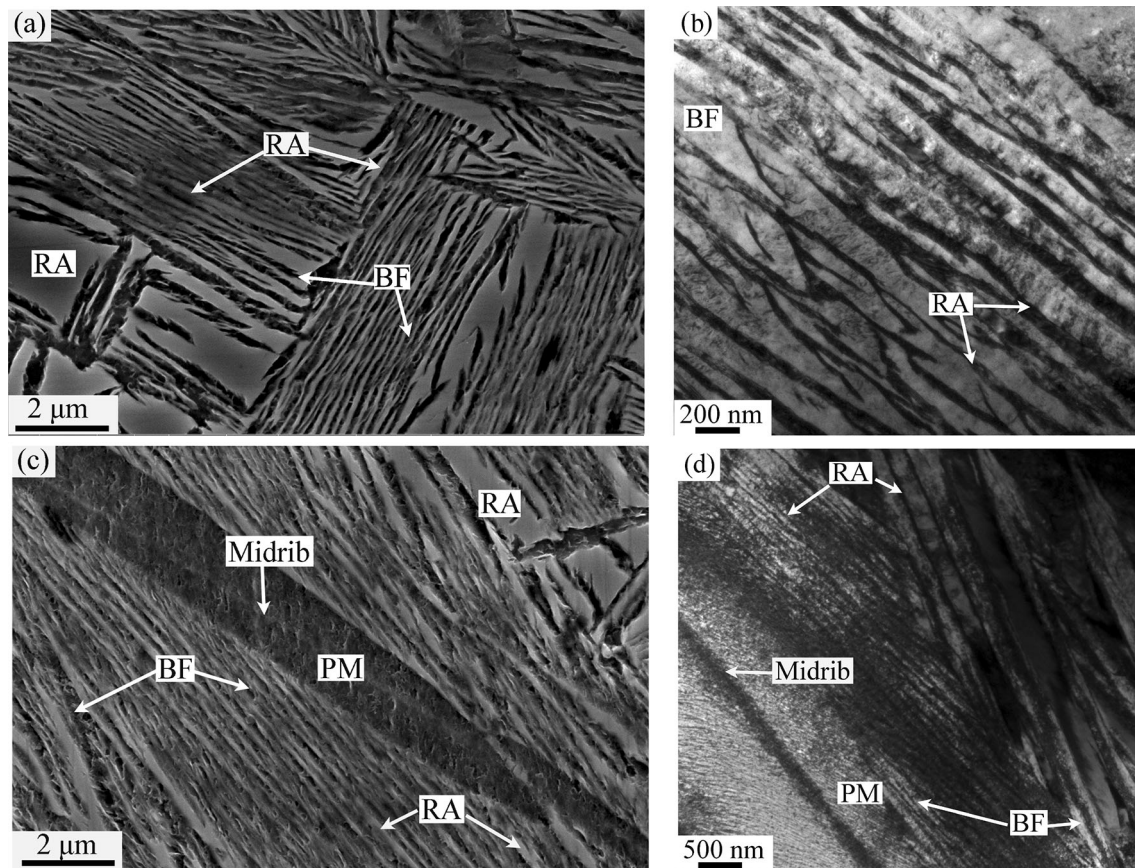


Fig. 3 Micrograph of specimens obtained by DBT process (a, b) and QBT process (c, d)

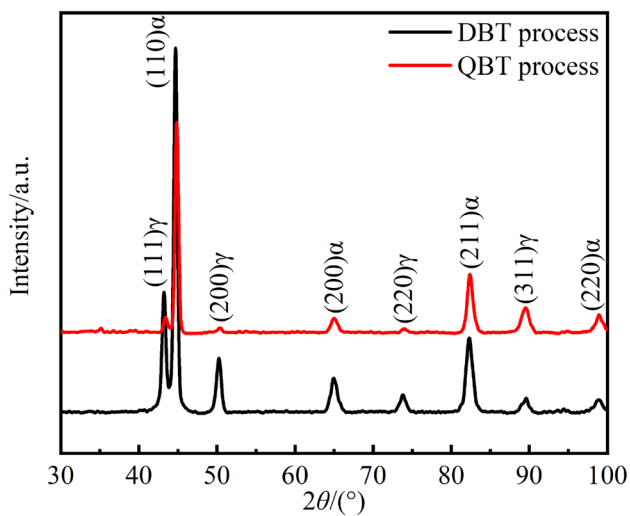


Fig. 4 XRD patterns of specimens treated by DBT and QBT processes

V_γ and C_γ of the specimens obtained by DBT and QBT processes were calculated and are listed in Table 2. The volume fraction of film-like ($V_{\gamma f}$) and blocky ($V_{\gamma b}$) retained austenite can also be calculated based on the proposal that the volume fraction of film-like retained austenite is almost

Table 2 Microstructural parameters of specimens subjected to DBT and QBT processes (%)

Process	V_γ	V_B	$V_{\gamma f}$	$V_{\gamma b}$	V_M	C_γ
DBT	26.7	73.3	11.0	15.7	–	1.44
QBT	22.0	65.4	9.8	12.2	12.6	1.54

V_B and V_M Volume fraction of bainite and martensite, respectively

15% of bainite microstructure in high-carbon bainitic steel [34, 35]. The results are presented in Table 2. The introduction of prior martensite reduces the volume fraction of retained austenite and increases the carbon content within it of the specimen manufactured by QBT process. The high-carbon content of retained austenite suggested the high mechanical stability during tensile test [28], which can improve the strength of high-carbon nano-bainitic steel.

Figure 5 shows the microstructural morphology of PM and adjacent bainite microstructure including BF plates and film-like RA, as well as the corresponding crystallographic orientation obtained by EBSD from the specimen fabricated by QBT process. The complete martensite grain and nearby bainite microstructure cannot be fully observed at

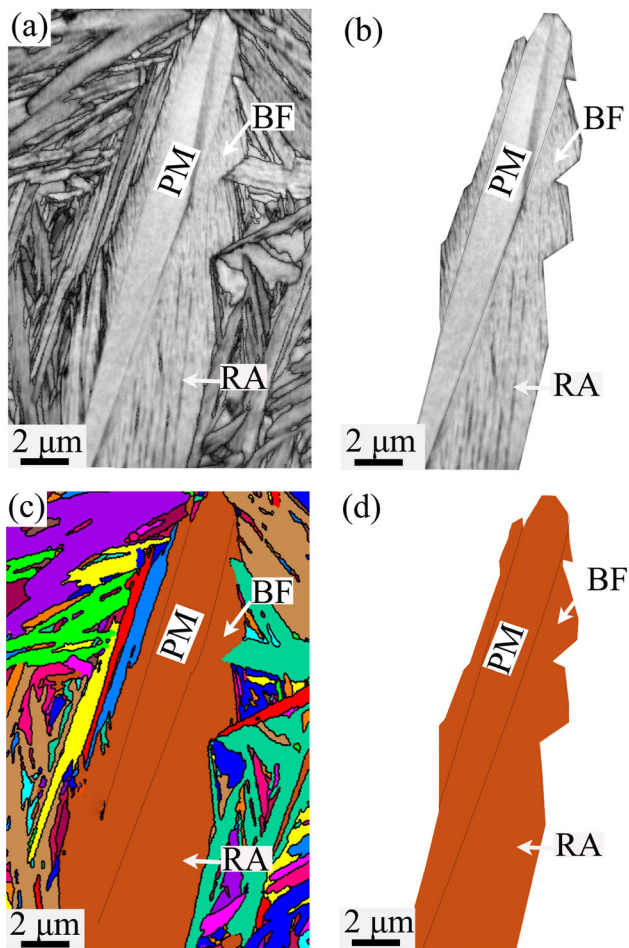


Fig. 5 SEM microstructure (a, b) and corresponding crystallographic orientation figure map (c, d) of specimen fabricated by QBT process

the same time, due to the large different size between the two phases. The orientation of bainitic ferrite and film-like retained austenite around martensite grain cannot be distinguished since the thickness of BF plates is thinner than the scanning step during EBSD measurements. Even so, the orientation relationship between prior martensite and adjacent bainite microstructure can be reflected representatively. As shown in Fig. 5c, d, martensite grain and adjacent bainitic ferrite plates show similar orientation. Yet, the bainite microstructure away from the prior martensite grain shows entirely different orientation relationship with the martensite grain. It should be noted that the zone of bainite microstructure that showed the same orientation with martensite grain overlaps with the microstructural refinement region. The experimental results suggest that the acceleration mechanism of bainite transformation by prior martensite may be that additional dislocation introduced into austenite matrix by martensite assists following bainite transformation [22, 30].

The parallelogram strain field with point symmetry in austenite matrix is formed due to the existence of prior

martensite. The ensured internal stresses relax through slip within the austenite matrix around the phase interface. On the one hand, the plastic deformation in the austenite matrix caused by stresses relaxation results in the similar orientation relationship between martensite and the adjacent bainite microstructure [24]; on the other hand, high density dislocations are also created in austenite during martensite transformation and act as the nucleation sites for the bainite transformation. Therefore, the bainite microstructure with the same orientation as the adjacent martensite grain is refined and the incubation time of bainite transformation is shortened obviously in QBT process. The other result of the microstructure refinement is that the peak value of transformation rate in QBT process is higher than that in DBT process. Since martensite grain with small volume fraction is formed in present work, the extra parallelogram strain field is limited to the vicinity of martensite. Moreover, the introduction of prior martensite refined the supercooled austenite matrix and then inhibited the subsequent growth of bainitic ferrite. Thus, the average transformation rate in QBT process is lower than that in DBT process, as shown in Fig. 2c.

3.3 Mechanical properties

The engineering stress–strain curves, true stress–strain curves, and work hardening rate curves of the high-carbon nano-bainitic steel are shown in Fig. 6. The mechanical properties of two specimens subjected to DBT and QBT processes were measured and are listed in Table 3. All the engineering stress–strain curves and true stress–strain curves of two specimens show continuous yielding behavior and significant work hardening; however, the specimen for QBT process exhibits higher strength and hardness than that obtained by DBT process. This is primarily attributed to the finer bainite microstructure and prior martensite formed in QBT process than in DBT process, as observed by SEM and TEM micrographs. The work hardening rate curves as shown in Fig. 6b reveal three stages of work hardening. The work hardening rate of DBT and QBT processes decreases with increasing strain in stage-I, which can be attributed to the high-density mobile dislocations in bainitic ferrite plates [36, 37]. The steeper slope of QBT process is related to the finer bainite microstructure that inhibits the movement of dislocation during plastic deformation. Strain-induced martensite transformation occurs at the begin of stage-II [38, 39], resulting in a slight increase in work hardening rate for DBT and QBT processes. The larger increment of work hardening rate in DBT process can be attributed to the more retained austenite with lower carbon content. However, the retained austenite with higher carbon content of the specimen obtained by QBT process has better

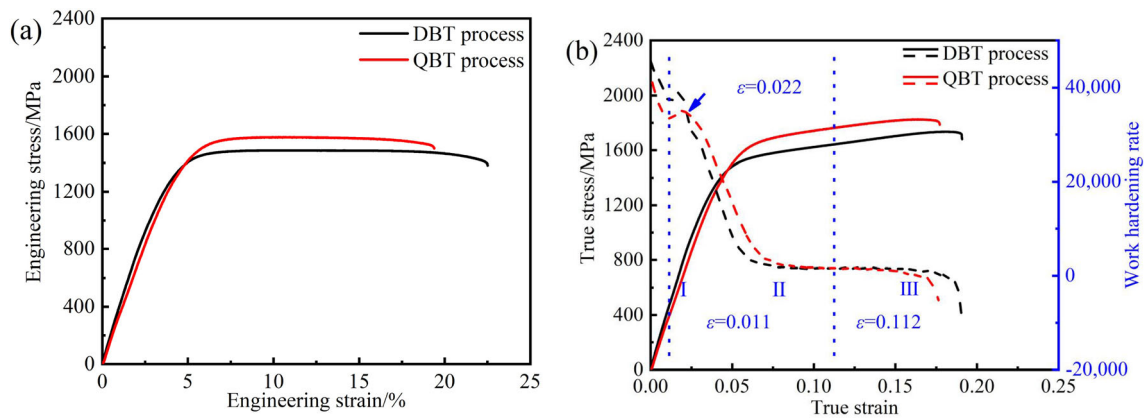


Fig. 6 Engineering stress–strain curves (a), as well as true stress–strain curves and work hardening rate curves (b) of specimens obtained by DBT process and QBT process

Table 3 Mechanical properties of specimens obtained by DBT and QBT processes

Process	R_m / MPa	R_e / MPa	Elongation/ %	α_{KV} / ($J\ cm^{-2}$)	Hardness/ HV
DBT	1447	1110	24.3	13.1	496 ± 2.9
QBT	1522	1220	21.2	22.7	530 ± 5.3

R_m Ultimate tensile strength; R_e yield strength; α_{KV} V-notched impact toughness

mechanical stability and the specimen shows higher work hardening rate than the specimen obtained by DBT process when the true strain (ϵ) exceeds 0.022. A significant decrease in work hardening rate in stage-II can be explained by the fact that volume expansion caused by martensite formation during tensile deformation is restrained by the adjacent bainite microstructure [40]. All the retained austenite has transformed into martensite at the end of stage-II, and then, the work hardening rate curves exhibit a platform. Stage-III presents the deformation of all the microstructures including bainitic ferrite, retained austenite, and martensite. The strain incompatibility at the interface between bainite microstructure and prior martensite can lead to a larger reduction in work hardening rate in QBT process after the true strain is over 0.112 [41].

Furthermore, the impact toughness of the specimen obtained by QBT process is nearly twice that by DBT process. Factors including size of bainite microstructure, volume fraction of blocky retained austenite, and the carbon content within it influence the impact toughness of the nano-bainitic steel. Firstly, the refined bainite microstructure, especially the refined film-like retained austenite, and the presence of prior martensite obtained by QBT process should be responsible for the obviously increased impact toughness of nano-bainitic steel. Secondly, although the

cracks tend to propagate along the interface between prior martensite and retained austenite, and the low angle grain boundaries have little resistance to crack propagation [42], the ultra-fine bainite microstructure including nanoscale bainitic ferrite plates and film-like retained austenite around prior martensite can inhibit the propagation of crack. Lastly, larger blocky retained austenite in specimens with DBT process tends to mechanically transform into blocky martensite, which is easy to become the origin of cracks and the paths of crack propagation, whereas in specimens with QBT process, smaller blocky and thin film-like retained austenite with higher carbon content increases the toughness by absorbing microcracks [43].

4 Conclusions

1. Compared to DBT process, the incubation time of bainite transformation in QBT process is shortened obviously from 702.0 to 57.6 s. The peak value of transformation rate in QBT process is higher than that in DBT process, and the occurrence time is earlier in QBT process than in DBT process, indicating that both the incubation time and growth stage of bainite transformation can be shortened by the presence of prior martensite.
2. On the one hand, the plastic deformation caused by the prior martensite transformation rotates the austenite matrix and results in the similar orientation relationship between final bainite microstructure and prior martensite. On the other hand, dislocations are also created due to the strain release and can act as the nucleation sites for bainite transformation. Therefore, the bainite microstructure adjacent to martensite is refined and the bainite transformation is accelerated.
3. The strength and hardness of the specimen prepared by QBT process are higher than those by DBT process,

due to the refined bainite microstructure and prior martensite obtained through QBT process. Although the presence of prior martensite and low misorientation relationship between the martensite and bainite microstructure is beneficial to crack propagation, the nanoscale bainitic ferrite plates and film-like retained austenite can inhibit the crack propagation and then improve the impact toughness of the high-carbon nano-bainitic steel.

Acknowledgements The authors gratefully acknowledge the support of the National Natural Science Foundation of China (Grant No. 51774033) and Innovative Talents Fund Gold Project from University of Science and Technology Beijing.

References

- [1] H.K.D.H. Bhadeshia, *Sci. Technol. Adv. Mater.* 14 (2013) 014202.
- [2] F.C. Zhang, B. Lv, C.L. Zheng, Q. Zou, M. Zhang, M. Li, T.S. Wang, *Wear* 268 (2010) 1243–1249.
- [3] F.G. Caballero, M.J. Santofimia, C. Garcia-Mateo, J. Chao, C. Garcia de Andres, *Mater. Des.* 30 (2009) 2077–2083.
- [4] C. Garcia-Mateo, F.G. Caballero, H.K.D.H. Bhadeshia, *ISIJ Int.* 43 (2003) 1238–1243.
- [5] Q.H. Pang, M. Xu, Z.L. Mi, J. Cui, J. Guo, *J. Iron Steel Res. Int.* 28 (2021) 66–75.
- [6] F. Zhen, K. Zhang, Z.L. Guo, J.B. Qu, *J. Iron Steel Res. Int.* 22 (2015) 645–651.
- [7] J. Mahieu, S. Claessens, B.C. De Cooman, *Metall. Mater. Trans. A* 32 (2001) 2905–2908.
- [8] P. Pointner, *Wear* 265 (2008) 1373–1379.
- [9] J. Chakraborty, D. Bhattacharjee, I. Manna, *Scripta Mater.* 59 (2008) 247–250.
- [10] T.S. Wang, X.Y. Li, F.C. Zhang, Y.Z. Zheng, *Mater. Sci. Eng. A* 438–440 (2006) 1124–1127.
- [11] J. Yang, T.S. Wang, B. Zhang, F.C. Zhang, *Mater. Des.* 35 (2012) 170–174.
- [12] C. Garcia-Mateo, F.G. Caballero, H.K.D.H. Bhadeshia, *ISIJ Int.* 43 (2003) 1821–1825.
- [13] E.V. Pereloma, I.B. Timokhina, M.K. Miller, P.D. Hodgson, *Acta Mater.* 55 (2007) 2587–2598.
- [14] H.J. Hu, H.S. Zurob, G. Xu, D. Embury, G.R. Purdy, *Mater. Sci. Eng. A* 626 (2015) 34–40.
- [15] S. Glochin, B. Avishan, S. Yazdani, *Mater. Sci. Eng. A* 656 (2016) 94–101.
- [16] J.Y. Meng, Y. Feng, Q. Zhou, L.J. Zhao, F.C. Zhang, L.H. Qian, *J. Mater. Eng. Perform.* 24 (2015) 3068–3076.
- [17] A. Kumar, A. Singh, *Mater. Sci. Eng. A* 729 (2018) 439–443.
- [18] R. Bakhtiari, A. Ekrami, *Mater. Sci. Eng. A* 525 (2009) 159–165.
- [19] L.J. Zhao, L.H. Qian, J.Y. Meng, Q. Zhou, F.C. Zhang, *Scripta Mater.* 112 (2016) 96–100.
- [20] J. Feng, T. Frankenbach, M. Wettlaufer, *Mater. Sci. Eng. A* 683 (2017) 110–115.
- [21] S.L. Xia, F.C. Zhang, Z.N. Yang, *Mater. Sci. Eng. A* 724 (2018) 103–111.
- [22] W. Gong, Y. Tomota, S. Harjo, Y.H. Su, K. Aizawa, *Acta Mater.* 85 (2015) 243–249.
- [23] C.H. Chu, Y.M. Qin, X.M. Li, Z.N. Yang, F.C. Zhang, C.H. Guo, X.Y. Long, L.L. You, *Materials* 12 (2019) 166.
- [24] G. Miyamoto, A. Shibata, T. Maki, T. Furuhashi, *Acta Mater.* 57 (2009) 1120–1131.
- [25] H. Kawata, K. Hayashi, N. Sugiura, N. Yoshinaga, M. Takahashi, *Mater. Sci. Forum* 638–642 (2010) 3307–3312.
- [26] B. Kim, C. Celada, D. San Martín, T. Sourmail, P.E.J. Rivera-Díaz-del-Castillo, *Acta Mater.* 61 (2013) 6983–6992.
- [27] D.J. Dyson, B. Holmes, *J. Iron Steel Inst.* 208 (1970) 469–474.
- [28] X.C. Xiong, B. Chen, M.X. Huang, J.F. Wang, L. Wang, *Scripta Mater.* 68 (2013) 321–324.
- [29] Y. Toji, H. Matsuda, D. Raabe, *Acta Mater.* 116 (2016) 250–262.
- [30] A. Shibata, S. Morito, T. Furuhashi, T. Maki, *Scripta Mater.* 53 (2005) 597–602.
- [31] L.J. Zhao, L.H. Qian, Q. Zhou, D.D. Li, T.L. Wang, Z.G. Jia, F.C. Zhang, J.Y. Meng, *Mater. Des.* 183 (2019) 108123.
- [32] C. Garcia-Mateo, F.G. Caballero, *Mater. Trans.* 46 (2005) 1839–1846.
- [33] H. Guo, A. Zhao, R. Ding, C. Zhi, J. He, *Mater. Sci. Technol.* 32 (2016) 1605–1612.
- [34] H.K.D.H. Bhadeshia, D.V. Edmonds, *Met. Sci.* 17 (1983) 420–425.
- [35] B. Avishan, S. Yazdani, F.G. Caballero, T.S. Wang, C. Garcia-Mateo, *Mater. Sci. Technol.* 31 (2015) 1508–1520.
- [36] A. Barbacki, *J. Mater. Process. Technol.* 53 (1995) 57–63.
- [37] N.K. Balliger, T. Gladman, *Met. Sci.* 15 (1981) 95–108.
- [38] S. Das, S. Sinha, A. Lodh, A.R. Chintla, M. Krugla, A. Haldar, *Mater. Sci. Technol.* 33 (2017) 1026–1037.
- [39] A. Kumar, S.B. Singh, K.K. Ray, *Mater. Sci. Eng. A* 474 (2008) 270–282.
- [40] S.M. Hasan, A. Mandal, S.B. Singh, D. Chakabarti, *Mater. Sci. Eng. A* 751 (2019) 142–153.
- [41] T.S. Byun, I.S. Kim, *J. Mater. Sci.* 28 (1993) 2923–2932.
- [42] P. Zhou, B. Wang, L. Wang, Y. Hu, L. Zhou, *Mater. Sci. Eng. A* 722 (2018) 112–121.
- [43] Q. Zhou, L.H. Qian, J. Tan, J.Y. Meng, F.C. Zhang, *Mater. Sci. Eng. A* 578 (2013) 370–376.